ADVANCED MATERIALS

DOI: 10.1002/adma.200502194

Size-Dependent Transport and Thermoelectric Properties of Individual Polycrystalline Bismuth Nanowires**

By *Akram Boukai*, *Ke Xu*, and *James R. Heath**

Thermoelectric materials convert a temperature difference into electricity and vice versa.[1–3] Such materials utilize the Seebeck effect for power generation and the Peltier effect for cooling. In the Seebeck effect, a temperature difference across a material causes the diffusion of charged carriers across that gradient, thus creating a voltage difference between the hot and cold ends of the material. Conversely, the Peltier effect explains the fact that when current flows through a material a temperature gradient arises because the charged carriers exchange thermal energy. Thermoelectrics perform these functions without moving parts or toxic gases, which make them unique among power generation and cooling methods. Presently, thermoelectrics find only limited use because of their poor efficiency.

The efficiency of a thermoelectric material is determined by the dimensionless figure of merit

$$ZT = \frac{S^2\sigma}{\kappa}T \qquad (1)$$

where S is the thermoelectric power, defined as the thermoelectric voltage (V_p) produced per degree temperature difference ($S = dV_p/dT$), σ is the electrical conductivity, κ is the thermal conductivity, and T is the temperature.[4,5] To maximize ZT, S must be large so that a small temperature difference can create a large voltage, σ must be large in order to minimize joule heating losses, and κ must be small to reduce heat leakage and maintain a temperature difference. S, σ, and κ are not, however, mutually exclusive.[6,7] For instance, in a bulk material, the Weidmann–Franz law limits the ratio σ/κ. Also, a sharply peaked density of states favors large S, but the density of states is a smoothly varying function for bulk materials.[8,9] Dresselhaus' group has suggested that 1D nanowires yield improved thermoelectric efficiencies.[10,11]

Bismuth has a small effective mass ($0.001\,m_0$ along the trigonal direction), large thermoelectric power ($50\ \mu V\,K^{-1}$ to $100\ \mu V\,K^{-1}$), and small thermal conductivity ($8\ W\,m^{-1}\,K^{-1}$), all of which help increase ZT.[11] For bulk Bi, ZT is limited because the conduction and valence bands indirectly overlap (~38 meV), which causes Bi to be a compensated semimetal,[12] meaning that the contributions of holes and electrons to S cancel each other. However, a semimetal-to-semiconductor transition has been predicted for Bi nanowires below a critical size (~50 nm depending on the crystal orientation) due to the quantum-confinement effect.[11,13] Therefore, S is predicted to be significantly enhanced for Bi nanowires (NWs) with optimized position of the Fermi energy. 1D semiconductors are also characterized by a sharply peaked density of states.[8,9] Experimental evidence of the enhancement of S has been reported in Bi nanocomposites.[14] A Bi nanowire will also have a reduced κ due to phonon scattering off the sidewalls which helps increase ZT.[11,15]

Owing to its chemical instability and low melting point (~271 °C), fabrication and electric measurements of Bi nanowires are challenging. Embedded nanowire arrays have been prepared in porous templates by various methods.[16–18] Transport properties of such embedded NWs are limited to two-point resistance measurements,[17–24] with the numbers of wires measured being indeterminate.[25,26] Fewer measurements on the thermoelectric power of Bi nanowire arrays have been reported.[23,24] In addition, the very small thicknesses of the embedded NW samples leads to an underestimate of S because the thermocouples used to measure the temperature are comparable to the sample thickness.[25]

We have overcome several of these limitations by coupling a device architecture used by Small et al.[27] and Llaguno et al.[28] for nanotube studies with nanofabrication steps that are compatible with the material limitations of bismuth. This resulting device provides a reliable four-point electrical-conductivity measurement, allows for accurate measurements of thermoelectric power, and permits quantitation of electric and magnetic field effects on the transport of individual Bi NWs.

Figure 1a shows one of our devices. The outer electrodes pass a current through the NWs, while the inner two sets serve as voltage probes for the four-point measurements and the thermoelectric-voltage measurements. A current passed through a heater locally heats the SiO_2, resulting in a temperature gradient (and thermoelectric voltage) along the Bi NWs. The thermoelectric voltage is detected from the inner two sets of electrodes with a Keithley 2182 nanovoltmeter

[*] Prof. J. R. Heath, A. Boukai, K. Xu
Division of Chemistry and Chemical Engineering
California Institute of Technology
MC 127-72, 1200 East California Blvd., Pasadena, CA 91125 (USA)
E-mail: heath@caltech.edu

[**] Akram Boukai and Ke Xu contributed equally to this work. This work was supported by the Department of Energy and by the MARCO Center for Advanced Materials and Devices. We would also like to acknowledge Dr. Ezekiel Johnston-Halperin and Dr. Yi Luo for fabrication assistance and advice.

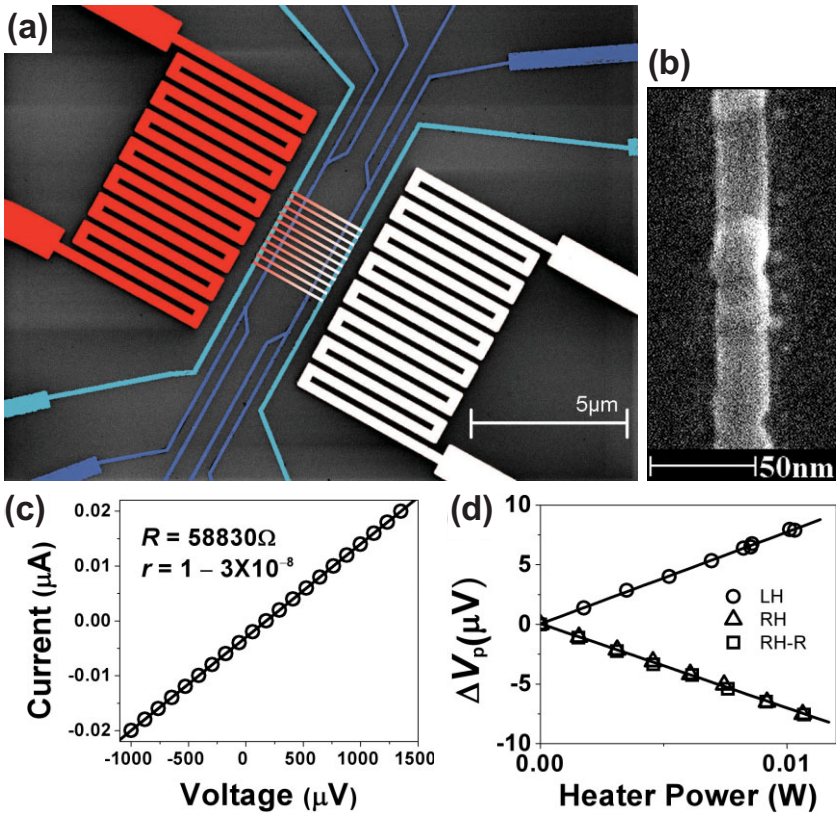

Figure 1. a) A false-color scanning electron microscopy image of a typical device used in this study. The left heater is shown in red, the right heater in white, and the 11 Bi NWs are shown as a red → white gradient. The inner (dark blue) electrodes are used for temperature measurements and, with the outer (light blue) electrodes, are used for four-point conductivity measurements of the NWs. b) A small section of a 28 nm Bi NW investigated in this study. c) A typical (28 nm Bi NW; 300 K) four-point current–voltage curve obtained from the device, showing Ohmic conductivity. Four-point resistance R is obtained from a linear fit with correlation coefficient r indicated. d) A typical (28 nm Bi NW device; 300 K) thermoelectric voltage response ΔV_p measured on the device as a function of heating power for the left heater (LH), right heater (RH), and right heater with a reversed current direction (RH-R).

(impedance >10 GΩ) as a function of the heater power (Fig. 1d). The temperature difference between these inner electrodes is calibrated to the heater power by monitoring the respective changes in their four-point resistance when changing the heater power or system temperature (within 4 K). The calibration is performed on every device for each temperature point that the thermoelectric power is measured. The highly doped Si substrate underneath the SiO_2 serves as a gate electrode for electric field-effect measurements.

Care was taken to eliminate possible experimental artifacts. For four-point resistance measurements, current–voltage (I–V) curves (Fig. 1c) are always obtained with good linearity, confirming ohmic conductivity of the NWs. The resistance is obtained from the slope rather than a single-point I–V calculation to avoid possible influences from offset voltages. For thermoelectric measurements, either of the heaters is turned on right after re-zeroing the nanovoltmeter, and the voltage change ΔV_p is recorded as the thermoelectric voltage after the system has reached thermal equilibrium. ΔV_p originates from the temperature gradient caused by local heating based on the observations that ΔV_p increases linearly with the increase of heater power (square of the current), and that a reversed direction of current in the heater (which produces the same joule heat) does not change ΔV_p. Finally, passing a current through the heater on the other side of the NWs produces a comparable ΔV_p, but with opposite sign (Fig. 1d).

Bulk Bi has a screening length of 30 ~ 40 nm.[29–31] Although lower carrier concentrations in low-dimensional systems might be expected,[11] experiments have revealed carrier concentrations higher than the bulk value in Bi thin films[32] and NWs,[33] which would reduce the screening length. To ensure that the nanowires are thinner than the screening length, the smallest thickness (15 nm) that did not lead to discontinuous wires was used.

Attempts to extract embedded Bi NWs for four-point measurements have had limited success.[26,34] Four-point measurements for Bi NWs thinner than 70 nm have not, to our knowledge, been reported. Similarly, temperature-dependent four-point resistance of any Bi NWs has not been reported due to the difficulty in establishing ohmic contacts.[26] We obtained linear I–V curves (Fig. 1c) from 1.7–300 K, demonstrating that we achieved good ohmic contacts.

Resistivity of the NWs can be calculated from the four-point resistance since the NW dimensions and numbers of NWs measured are both known. The resistivities at 300 K are 13, 9.5, 55, and 66 μΩm for cross sections of 15 nm by 72, 55, 40, and 28 nm, respectively, which corresponds to resistivities 10, 7, 42, and 50 times of that of bulk Bi. The increase of resistivity for thinner Bi wires reflects greater contributions from boundary and surface scatterings. A previously reported four-point measurement on a 70 nm diameter NW prepared from template-assisted growth yielded a resistivity six times greater than that of bulk Bi.[26]

The temperature-dependent resistance is given in Figure 2a. The observed trends generally agree with two-point measurements on vapor-deposited Bi nanowire arrays:[20] The widest

ADVANCED MATERIALS

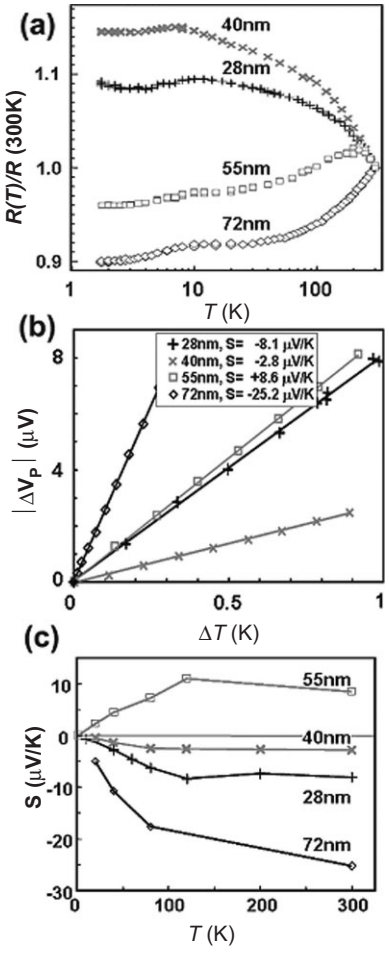

Figure 2. Electrical transport and thermoelectric properties of Bi nanowires. a) The temperature dependent resistance of Bi NWs, normalized to the resistance at 300 K. Each point in the plot is obtained by fitting a four-point *I*–*V* trace. b) Absolute values of measured thermoelectric voltage of Bi NWs at 300 K as a function of temperature difference across the nanowires. Thermoelectric power *S* is obtained from the slope of a linear fit to the data. (Note: 55 nm NWs yielded a positive thermoelectric power while others gave a negative thermoelectric power.) c) Thermoelectric power *S* as a function of temperature for different NWs.

wires yield bulklike semimetal behavior, while the resistance for the thinnest two sets of NWs increases monotonically with decreasing temperature. The 55 nm wires exhibit an intermediate behavior. These trends have been cited as evidence that a quantum-confinement-induced semimetal-to-semiconductor transition occurs when the wire width decreases below about 50 nm,[21,25] consistent with theoretical predictions.[11] However, separating changes in carrier density and carrier mobility is inherently difficult.[33] Our electric-field-effect measurements (see below) suggest the 40 nm wide NWs are still semimetallic. Consequently, the observed trends may reflect a decreased mobility through surface and grain-boundary scattering.[21]

A resistance drop is observed below 10 K in all devices. This is reminiscent of the reported superconducting transition of amorphous Bi films around 6 K,[35,36] and may imply the existence of amorphous regions within the polycrystalline structure. We found that the drop disappears when a strong magnetic field is applied, which presumably quenches the superconducting transition.

The thermoelectric voltage and power measurements on the Bi NWs are shown in Figures 2b and c. Figure 2b demonstrates the linearity of the thermoelectric voltage measured with respect to the applied temperature difference, indicating $S = dV_p/dT$ is a constant. The measured S is really that of the NW/electrode couple since it contains a contribution from the thermoelectric power of the metal electrodes, S_m. However, the S of Pt and Ti tend to cancel each other and are both within $\pm 5\ \mu V\,K^{-1}$ at all temperatures studied here.[37] The trend of Figure 2c in which S (for all NWs) is relatively temperature invariant above 100 K has been observed in essentially all reported measurements on bulk,[38] thin-film,[39] and thin-wire[23,24] bismuth. The magnitude of S for all NWs tends to zero as the temperature is decreased. S is also the entropy per electric charge, and so must go to zero at 0 K.

The 72 nm wide NWs show the largest (room temperature) S of $-25.2\ \mu V\,K^{-1}$. This value is about one half of that of bulk Bi in the same direction (perpendicular to the trigonal axis),[40] but agrees with both earlier measurements of S ($-28\ \mu V\,K^{-1}$) of thin (33 nm) Bi films[40] and recent results ($-22\ \mu V\,K^{-1}$ and $-28\ \mu V\,K^{-1}$) on two NW arrays.[24] S is reduced dramatically for the smaller NWs. Both theory[41] and experiment[40] have concluded that surface and grain-boundary scattering will reduce S in polycrystalline thin films. This may also apply to the width of NWs.

For bulk Bi, and for the 72, 40, and 28 nm NWs, S is negative because electrons have a much higher mobility than holes and dominate the transport.[32,42] The 55 nm NW on the other hand shows a positive S (Fig. 2c) indicating p-type carrier-dominated transport, which has been reported in two Bi NW composites[14] and a 200 ± 50 nm Bi wire[43] before. Calculations based on the gating response of our NWs (see below) suggest that an impurity level of 10 ppm could be sufficient to change S from negative to positive.

Controlling the position of the Fermi energy (E_F) in order to enhance the thermoelectric power[25] may be achieved through doping or the electric-field effect (EFE).[31,44] Controlling the doping level to a precision of 10^{17} cm^{-3} (or 4 ppm of dopants) is desirable,[11] but hard to achieve experimentally.[21] For example, 99.999 % purity Bi has an impurity level of 10 ppm. However, our Bi NWs are thinner than the screening length,[44] thus enabling EFE measurements. The effective doping level (N_d) can be estimated based on the Si–SiO_2–Bi capacitance structure as a function of the gating voltage V_g

$$N_d = \frac{Q_d}{eV_{Bi}} = \frac{CV_g}{eAh_{Bi}} = \frac{\varepsilon_0\varepsilon_{r,SiO_2}\frac{A}{d_{SiO_2}}}{eAh_{Bi}}V_g = \frac{\varepsilon_0\varepsilon_{r,SiO_2}}{ed_{SiO_2}h_{Bi}}V_g \qquad (2)$$

where $\varepsilon_0\varepsilon_{r,SiO_2}$ is the permittivity of the SiO_2 layer, which serves as the dielectric medium, the thickness of the SiO_2

layer d_{SiO_2} is 500 nm, and the height of the Bi NWs h_{Bi} is 15 nm. From Equation 2 we obtain $N_d = 2.8 \times 10^{16}$ cm^{-3}/V $\cdot V_g$. Thus, the effective dopant concentration can be controlled to 10^{16} cm^{-3} or lower with appropriate V_g. Our devices functioned properly up to $V_g = \pm 150$ V, or an effective dopant concentration of 4×10^{18} cm^{-3}. This is sufficient for the thermoelectric optimization predicted by theory.[11] The EFE results of the 40 nm Bi NW device at 20 K are given in Figure 3. Ohmic conductivity was observed for all gating voltages, and the conductance (G) values were obtained from a linear fit to

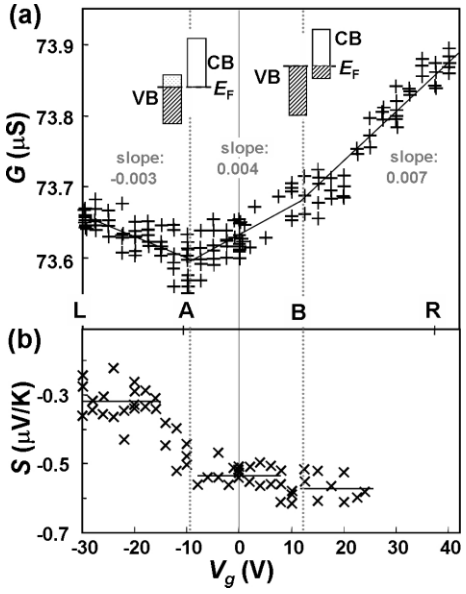

Figure 3. Measured four-point conductance G and thermoelectric power S versus gate voltage V_g for 40 nm Bi NWs at 20 K. G and S are measured separately during different scans, and data obtained from several scans with different scan directions and steps are integrated into a single plot to verify the trends are not due to drift. Schematic drawings of the possible positions of Fermi level at the turning points A and B are given along with the slopes of G (dG/dV_g) as a possible interpretation of the results (see text).

the I–V curves. Similar behavior has been observed in thin carbon films.[44]

The conductance and thermoelectric power trends in Figure 3, which were collected separately during several different scans to avoid possible drift, are found to be well correlated by the Mott formula, which relates the diffusive thermoelectric power, S_d, to the conductance G[45]

$$S_d = \frac{-\pi^2 k_B^2 T}{3|e|} \frac{1}{G} \frac{dG}{dE}\bigg|_{E=E_F} \quad (3)$$

An increase in V_g would put more electrons into the Bi nanowires and elevate E_F, i.e., dE_F/dV_g is positive. Consequently,

$$\frac{dG}{dV_g} = \frac{dE_F}{dV_g} \frac{dG}{dE}\bigg|_{E=E_F} \quad (4)$$

is expected to be of the same sign as

$$\frac{dG}{dE}\bigg|_{E=E_F} \quad (5)$$

and thus from Equation 2 S_d should have the opposite sign of dG/dV_g. The measured S clearly shows this trend: a sudden drop in the measured S is observed when the slope of G with respect to V_g changes from negative to positive at point A. This correlates to a change of positive S_d to negative S_d. Another decrease in S (and an increase in the slope of G) is observed around point B. It naturally follows that somewhere around point A (~–10 V), with a measured S of between –0.5 to –0.4 μV K^{-1}, should correspond to an S_d value of 0. The observed nonzero value of S is reflective of two facts: 1) S_g, the phonon-drag component of S, has not been taken into account, which could be significant at this temperature,[46] and 2) S_m, the thermoelectric power of Pt/Ti electrodes used to establish the thermocouple with Bi nanowires, has not been considered. The Pt/Ti electrodes are not expected to contribute to the EFE due to their extremely small screening lengths,[44] but they might cause a uniform shift $-S_m$ in S at all V_g.

40 nm Bi NWs have been predicted to be semiconductors at 20 K for any growth direction,[11] and results similar to Figure 2a has been cited as evidence of the semimetal-to-semiconductor transition around 55 nm.[21,23] Our EFE result, however, is found to be more readily explained with a semimetal model.[44] The two turning points A and B around ±10 V correspond to an effective dopant concentration of about $N_d = 3 \times 10^{17}$ cm^{-3}, which is close to the carrier concentrations measured in bulk (semimetal) Bi, $N_e \approx N_d = 2.5$–4×10^{17} cm^{-3}, obtained from various methods.[47,48] These two turning points are thus assigned to be when the Fermi level is at the bottom of the conduction band (A) and at the top of the valence band (B). If the bottom of conduction band is lower than the valence band as in a semimetal (see drawings in Fig. 3a), the observed results can be rationalized. According to the assignment, holes are the only carrier when $V_g < -10$ V, which results in positive S_d, and a decrease in G with increasing V_g, as the concentration of holes would decrease when putting more electrons in the nanowires. Similarly, electrons are the only carrier for $V_g > 10$ V, which results in negative S_d and an increase in G with increasing V_g. For $-10\ \text{V} < V_g < 10$ V, both electron and hole carriers (either extrinsic, intrinsic, or both) are present and contribute to the conductivity σ and thermoelectric power S

$$\sigma = \sigma_e + \sigma_h = e(N_e \mu_e + N_h \mu_h) \quad (6)$$

$$S = \frac{\sigma_e S_e + \sigma_h S_h}{\sigma_e + \sigma_h} = \frac{N_e \mu_e S_e + N_h \mu_h S_h}{N_e \mu_e + N_h \mu_h} \quad (7)$$

An increase in V_g in this region would cause an increase in N_e, the concentration of electrons, but a decrease in N_h, the concentration of holes.

ADVANCED MATERIALS

Consider the value of dG/dV_g (the slope of Fig. 3a) in the three regions L–A, A–B, and B–R. Note that $|\text{slope}|_{B-R} > |\text{slope}|_{L-A}$. This is consistent with the higher mobility[32,42] electrons dominating the region B–R and holes dominating L–A. Also note that $\text{slope}_{A-B} \approx \text{slope}_{L-A} + \text{slope}_{B-R}$. This indicates that both electrons and holes participate in the charge transport in the region A–B. A more quantitative analysis of the results would require knowledge of the density of states (DOS), but the near-linear dependence of G over V_g in the different regions suggests a near-constant DOS, similar to what might be expected for a 2D system.[44] This is reasonable for a 15 nm × 40 nm cross-section wire, as the electronic de Broglie wavelength is 30–40 nm in Bi.[49]

Our EFE results suggest semimetal behavior for 40 nm Bi NWs, with electron- and hole-carrier concentrations comparable to bulk values, contradicting theoretical predictions that Bi nanowires thinner than 50 nm would become semiconducting at this temperature,[11] and that as a consequence the total carrier density for 40 nm NW at 20 K would decrease significantly to smaller than 10^{16} cm^{-3},[11] about 100 times smaller than the bulk value. This could stem from the polycrystalline nature of our NWs, since interface states would be expected to contribute to the total density of states near E_F. Similar conclusions have been drawn from recent Shubnikov–de Haas oscillation measurements on 30 nm Bi wires in terms of surface-induced charge carriers.[33] Our 28 nm NW device was found to give similar trends as the 40 nm NW device, but the data set was less complete.

In conclusion, nanofabrication methods and a device architecture have been combined to allow for four-point electric, thermoelectric, magnetic-field, and electric-field-effect measurements on individual Bi nanowires. No clear semimetal-to-semiconductor transition or enhancement in thermoelectric power has been observed, probably due to the polycrystalline nature of our NWs. We are working towards extending these measurements to smaller NWs[50] (10–20 nm wide) fabricated from single-crystal films.[51,52]

Experimental

Thin Pt/Ti (7 nm/3 nm) electrodes and Pt/Ti (50 nm/10 nm) heaters were fabricated on a thermal SiO_2-coated (500 nm thick) degenerately doped Si substrate by electron-beam lithography (EBL). As the last step, ~2 μm long NWs were defined across the Pt electrodes by EBL. 15 nm of bismuth (99.999 %, Puratronic, Alfa Aesar) was deposited by e-beam evaporation at room temperature at 0.5 Å s^{-1} and at a base pressure of $< 5 \times 10^{-7}$ Torr (1 Torr ~ 133 Pa). A 28 nm wide Bi NW is shown in Figure 1b. The NWs were polycrystalline with an in-plane grain size comparable to the wire width. XRD results on a 15 nm thick film show the (003) and (006) peaks of rhombohedral Bi, with grains aligning to the trigonal orientation normal to the substrate, but likely with arbitrary in-plane orientations [53]. Dimensions were measured by scanning electron microscopy (SEM) and atomic force microscopy (AFM).

The Bi NWs were extremely fragile due to their small size, low melting point, and chemical instability. They were easily broken by ambient static charges, and oxidation typically causes a 1 % increase of the measured four-point resistance for every hour of air exposure. Thus, the NWs were fabricated just prior to wire bonding and chip mounting. During these last steps, the device contacts were shorted through a guard ring that was disconnected right before the device was loaded into a helium-sealed thermostat. With this approach, the NWs remained intact, and no discernible increase of resistance was found during the course of the measurement period (a few weeks).

Received: October 13, 2005
Final version: December 27, 2005

[1] D. K. C. MacDonald, *Thermoelectricity: An Introduction to the Principles*, Wiley, New York **1962**.
[2] N. W. Ashcroft, N. D. Mermin, *Solid State Physics*, Saunders College, Fort Worth, TX **1976**.
[3] G. Mahan, B. Sales, J. Sharp, *Phys. Today* **1997**, *50*, 42.
[4] G. Chen, M. S. Dresselhaus, G. Dresselhaus, J. P. Fleurial, T. Caillat, *Int. Mater. Rev.* **2003**, *48*, 45.
[5] M. S. Dresselhaus, G. Dresselhaus, X. Sun, Z. Zhang, S. B. Cronin, T. Koga, *Phys. Solid State* **1999**, *41*, 679.
[6] F. J. DiSalvo, *Science* **1999**, *285*, 703.
[7] A. Majumdar, *Science* **2004**, *303*, 777.
[8] G. D. Mahan, J. O. Sofo, *Proc. Natl. Acad. Sci. USA* **1996**, *93*, 7436.
[9] T. E. Humphrey, H. Linke, *Phys. Rev. Lett.* **2005**, *94*, 096 601.
[10] L. D. Hicks, M. S. Dresselhaus, *Phys. Rev. B: Condens. Matter Mater. Phys.* **1993**, *47*, 16 631.
[11] Y. M. Lin, X. Z. Sun, M. S. Dresselhaus, *Phys. Rev. B: Condens. Matter Mater. Phys.* **2000**, *62*, 4610.
[12] Y. Liu, R. E. Allen, *Phys. Rev. B: Condens. Matter Mater. Phys.* **1995**, *52*, 1566.
[13] X. Sun, Z. Zhang, M. S. Dresselhaus, *Appl. Phys. Lett.* **1999**, *74*, 4005.
[14] J. P. Heremans, C. M. Thrush, D. T. Morelli, M. C. Wu, *Phys. Rev. Lett.* **2002**, *88*, 216 801.
[15] R. Venkatasubramanian, E. Siivola, T. Colpitts, B. O'Quinn, *Nature* **2001**, *413*, 597.
[16] Z. B. Zhang, J. Y. Ying, M. S. Dresselhaus, *J. Mater. Res.* **1998**, *13*, 1745.
[17] J. Heremans, C. M. Thrush, Z. Zhang, X. Sun, M. S. Dresselhaus, J. Y. Ying, D. T. Morelli, *Phys. Rev. B: Condens. Matter Mater. Phys.* **1998**, *58*, R10 091.
[18] K. Liu, C. L. Chien, P. C. Searson, Y. Z. Kui, *Appl. Phys. Lett.* **1998**, *73*, 1436.
[19] Z. B. Zhang, X. Z. Sun, M. S. Dresselhaus, J. Y. Ying, J. P. Heremans, *Appl. Phys. Lett.* **1998**, *73*, 1589.
[20] J. Heremans, C. M. Thrush, Y. M. Lin, S. B. Cronin, Z. Zhang, M. S. Dresselhaus, J. F. Mansfield, *Phys. Rev. B: Condens. Matter Mater. Phys.* **2000**, *61*, 2921.
[21] Y. M. Lin, S. B. Cronin, J. Y. Ying, M. S. Dresselhaus, J. P. Heremans, *Appl. Phys. Lett.* **2000**, *76*, 3944.
[22] K. M. Hong, F. Y. Yang, K. Liu, D. H. Reich, P. C. Searson, C. L. Chien, F. F. Balakirev, G. S. Boebinger, *J. Appl. Phys.* **1999**, *85*, 6184.
[23] Y. M. Lin, O. Rabin, S. B. Cronin, J. Y. Ying, M. S. Dresselhaus, *Appl. Phys. Lett.* **2002**, *81*, 2403.
[24] J. Heremans, C. M. Thrush, *Phys. Rev. B: Condens. Matter Mater. Phys.* **1999**, *59*, 12 579.
[25] M. S. Dresselhaus, Y. M. Lin, S. B. Cronin, O. Rabin, M. R. Black, G. Dresselhaus, T. Koga, *Semicond. Semimetals* **2001**, *71*, 1.
[26] S. B. Cronin, Y. M. Lin, T. Koga, J. Y. Ying, M. S. Dresselhaus, *Mater. Res. Soc. Symp. Proc.* **2000**, *582*, H10.4.1.
[27] J. P. Small, K. M. Perez, P. Kim, *Phys. Rev. Lett.* **2003**, *91*, 256 801.
[28] M. C. Llaguno, J. E. Fischer, A. T. Johnson, J. Hone, *Nano Lett.* **2004**, *4*, 45.
[29] D. H. Brownell, E. H. Hygh, *Phys. Rev.* **1967**, *164*, 909.
[30] V. T. Petrashov, V. N. Antonov, B. Nilsson, *J. Phys.: Condens. Matter* **1991**, *3*, 9705.

[31] V. Sandomirsky, A. V. Butenko, R. Levin, Y. Schlesinger, *J. Appl. Phys.* **2001**, *90*, 2370.

[32] D. L. Partin, J. Heremans, D. T. Morelli, C. M. Thrush, C. H. Olk, T. A. Perry, *Phys. Rev. B: Condens. Matter Mater. Phys.* **1988**, *38*, 3818.

[33] T. E. Huber, A. Nikolaeva, D. Gitsu, L. Konopko, C. A. Foss, M. J. Graf, *Appl. Phys. Lett.* **2004**, *84*, 1326.

[34] S. B. Cronin, Y. M. Lin, O. Rabin, M. R. Black, J. Y. Ying, M. S. Dresselhaus, P. L. Gai, J. P. Minet, J. P. Issi, *Nanotechnology* **2002**, *13*, 653.

[35] W. Buckel, R. Hilsch, *Z. Phys.* **1954**, *138*, 109.

[36] J. S. Shier, D. M. Ginsberg, *Phys. Rev.* **1966**, *147*, 384.

[37] C. L. Foiles, in *Landolt–Börnstein—Group III Condensed Matter*, Vol. 15B, (Eds: K. H. Hellwege, J. L. Olsen), Springer, Berlin **1985**, p. 48.

[38] C. F. Gallo, B. S. Chandrasekhar, P. H. Sutter, *J. Appl. Phys.* **1963**, *34*, 144.

[39] S. Cho, A. DiVenere, G. K. Wong, J. B. Ketterson, J. R. Meyer, C. A. Hoffman, *Solid State Commun.* **1997**, *102*, 673.

[40] V. Damodara Das, N. Soundararajan, *Phys. Rev. B: Condens. Matter Mater. Phys.* **1987**, *35*, 5990.

[41] C. R. Pichard, C. R. Tellier, A. J. Tosser, *J. Phys. F: Met. Phys.* **1980**, *10*, 2009.

[42] A. H. Dekuijper, J. Bisschop, *Thin Solid Films* **1983**, *110*, 99.

[43] A. D. Grozav, E. Condrea, *J. Phys.: Condens. Matter* **2004**, *16*, 6507.

[44] K. S. Novoselov, A. K. Geim, S. V. Morozov, D. Jiang, Y. Zhang, S. V. Dubonos, I. V. Grigorieva, A. A. Firsov, *Science* **2004**, *306*, 666.

[45] M. Cutler, N. F. Mott, *Phys. Rev.* **1969**, *181*, 1336.

[46] M. W. Wu, N. J. M. Horing, H. L. Cui, *Phys. Rev. B: Condens. Matter Mater. Phys.* **1996**, *54*, 5438.

[47] J. P. Michenau, J. P. Issi, *J. Phys. C: Solid State Phys.* **1972**, *5*, 3061.

[48] G. A. Williams, *Phys. Rev.* **1965**, *139*, A771.

[49] N. Garcia, M. Strongin, Y. H. Kao, *Phys. Rev. B* **1972**, *5*, 2029.

[50] N. A. Melosh, A. Boukai, F. Diana, B. Gerardot, A. Badolato, P. M. Petroff, J. R. Heath, *Science* **2003**, *300*, 112.

[51] F. Y. Yang, K. Liu, K. M. Hong, D. H. Reich, P. C. Searson, C. L. Chien, *Science* **1999**, *284*, 1335.

[52] S. H. Choi, K. L. Wang, M. S. Leung, G. W. Stupian, N. Presser, B. A. Morgan, R. E. Robertson, M. Abraham, E. E. King, M. B. Tueling, S. W. Chung, J. R. Heath, S. L. Cho, J. B. Ketterson, *J. Vac. Sci. Technol., A* **2000**, *18*, 1326.

[53] J. Chang, H. Kim, J. Han, M. H. Jeon, W. Y. Lee, *J. Appl. Phys.* **2005**, *98*, 023 906.

